Afro-Asian Journal of Scientific Research (AAJSR)
المجلة الأفروآسيوية للبحث العلمي
E-ISSN: 2959-6505
Volume 4, Issue 2, 2026
Page No: 241-253
Website: https://aajsr.com/index.php/aajsr/index
SJIFactor 2024: 5.028 ISI 2025: 0.915 معامل التأثير العربي (AIF) 2025: 0.76

Synergistic Integration of Raman Spectroscopy and Artificial Intelligence for Precision Diagnostics and Theranostics in Breast Cancer

Nadir Omar Massoud Driza[1*], Hanan Mohammed Abdulsalam Ali[2], Ola Mohammed Ibrahim[3], Rafa Saad Abdulsalam Hamad[4], Huda Nadir Driza[5]
[1,2,3,4]Department of Physics and Medical Physics Department, Faculty of Arts and Sciences, University of Benghazi, Elmarj, Libya.
[5]Faculty of Medicine Al-Marj, University of Benghazi, Libya.

التكامل التآزري بين مطيافية رامان والذكاء الاصطناعي للتشخيص الدقيق والعلاج التشخيصي في سرطان الثدي

نادر عمر مسعود ادريزه[1*]، حنان محمد عبد السلام علي[2]، علا محمد إبراهيم[3]، رافع سعد عبد السلام حمد[4]، هدى نادر ادريزه[5]
[1،2،3،4]قسم الفيزياء، كلية الآداب والعلوم، جامعة بنغازي، المرج، ليبيا
[5]كلية الطب، جامعة بنغازي، المرج، ليبيا

*Corresponding author: nadir.driza@uob.edu.ly

Received: March 04, 2026	Accepted: April 24, 2026	Published: May 02, 2026

Abstract:
Breast cancer diagnostics are currently hampered by the qualitative nature of histopathology and the lack of real-time molecular specificity in standard imaging. Raman spectroscopy (RS) provides a superior alternative by leveraging the physics of inelastic photon scattering to perform label-free, non-destructive optical biopsies. When monochromatic laser light interacts with tissue, it undergoes a frequency shift corresponding to the specific vibrational energy levels of molecular bonds, such as $C-H$ bending in lipids (1445 cm-1), $C=O$ stretching (1745 cm-1), and Amide I $C=O$ stretching in proteins (1655 cm-1). This creates a high-dimensional biochemical "fingerprint" that precisely maps the transition from healthy adipose tissue to malignant stroma, characterized by a distinct drop in lipid-to-protein ratios and a surge in nucleic acid density (1330 cm-1). To resolve these subtle spectral shifts from the dominant fluorescence background, the integration of Artificial Intelligence (AI), specifically Convolutional Neural Networks (CNN) and Support Vector Machines (SVM), has proven essential for automated signal deconvolution and feature extraction. Clinical validations at institutions such as the University of Texas Southwestern and the University of Birmingham demonstrate that AI-augmented Raman systems achieve diagnostic accuracies exceeding 90%, offering a robust physical framework to replace time-intensive frozen sections and standardize intraoperative margin assessment. By digitizing the vibrational mechanics of the tumor microenvironment, RS coupled with AI represents the most powerful frontier in precision optical diagnostics.

Keywords: Raman Spectroscopy, Artificial Intelligence (AI), Breast Cancer Diagnostics, Deep Learning (DL), Machine Learning (ML).

الملخص:
تُواجه تشخيصات سرطان الثدي حاليًا تحديات تتمثل في الطبيعة النوعية لعلم الأمراض النسيجي (Histopathology) وعدم توفر خصوصية جزيئية آنية في تقنيات التصوير القياسية. ويوفر التحليل الطيفي رامان (Raman Spectroscopy - RS) بديلاً متفوقًا من خلال الاستفادة من فيزياء تشتت الفوتونات غير المرن لإجراء خزعات بصرية غير إتلافية ودون الحاجة إلى واسمات (Label-Free). فعندما يتفاعل ضوء ليزر أحادي اللون مع الأنسجة، فإنه يتعرض لانزياح في التردد يتوافق مع مستويات الطاقة الاهتزازية المحددة للروابط الجزيئية، مثل انحناء روابط C-H في الدهون (1445 سم⁻¹)، واستطالة روابط C=O (1745 سم⁻¹)، واستطالة رابطة C=O في نطاق الأميد الأول (Amide I) في البروتينات (1655 سم⁻¹). ويؤدي ذلك إلى تكوين (بصمة كيميائية حيوية) عالية الأبعاد ترسم بدقة الانتقال من الأنسجة الدهنية السليمة إلى السدى الخبيثة (Malignant Stroma)، والتي تتميز بانخفاض واضح في نسبة الدهون إلى البروتينات وارتفاع كثافة الأحماض النووية (1330 سم⁻¹). ولمعالجة هذه التحولات الطيفية الدقيقة وتمييزها عن الخلفية الفلورية المهيمنة، أثبت دمج الذكاء الاصطناعي (Artificial Intelligence - AI)، وبالتحديد الشبكات العصبية الالتفافية (Convolutional Neural Networks - CNN) وآلات المتجهات الداعمة (Support Vector Machines - SVM)، أهميته الكبيرة في إزالة تداخل الإشارات واستخلاص الخصائص بصورة آلية. وتُظهر الدراسات السريرية في مؤسسات مثل جامعة تكساس ساوثويسترن وجامعة برمنغهام أن أنظمة رامان المعززة بالذكاء الاصطناعي تحقق دقة تشخيصية تتجاوز 90%، مما يوفر إطارًا فيزيائيًا قويًا يمكن أن يحل محل المقاطع المجمدة التقليدية المستهلكة للوقت، ويسهم في توحيد تقييم الهوامش الجراحية أثناء العمليات. ومن خلال رقمنة الميكانيكا الاهتزازية للبيئة الدقيقة للورم، يمثل التحليل الطيفي رامان المقترن بالذكاء الاصطناعي أحد أقوى الآفاق المستقبلية في مجال التشخيصات البصرية الدقيقة.

الكلمات المفتاحية: مطيافية رامان، الذكاء الاصطناعي، تشخيص سرطان الثدي، التعلم العميق، التعلم الآلي.

Introduction:

Breast cancer constitutes a leading cause of oncological mortality among females globally, with 2.3 million new diagnoses and 670,000 deaths recorded in 2022. Established diagnostic modalities, including mammography, ultrasound, and histopathology, often present limitations such as elevated false-positive rates and a degree of inherent subjectivity. These factors can necessitate unnecessary biopsies and contribute to a deficiency in real-time intraoperative guidance. In breast-conserving surgical procedures, for instance, an estimated 20–30% of patients subsequently undergo re-excision due to the inability of conventional frozen sections to furnish immediate, definitive assessments of tumor margins [1] [2].

Raman Spectroscopy (RS) offers a promising approach to mitigate these challenges. This technique capitalizes on the principles of inelastic photon scattering to facilitate non-destructive, label-free optical biopsies. When monochromatic laser light, typically at wavelengths of 785 nm or 830 nm [3], interacts with biological tissue, it probes the distinct vibrational energy levels of molecular bonds. The resulting frequency shift, termed the "Raman shift," provides a characteristic biochemical signature, indicative of the intrinsic molecular composition within the tissue microenvironment, particularly in tumor contexts.
Within malignant breast tissue, the vibrational mechanics exhibit distinctive transformations. Healthy adipose tissue, for example, is primarily characterized by peaks associated with lipids, such as CH_2 deformation (1445 cm^{-1}) and $C = O$ stretching (1745 cm^{-1}). In contrast, invasive ductal carcinoma (IDC) typically displays a notable reduction in these lipid signals, often attributed to their displacement by a denser tumor stroma. This shift is concurrently observed with an increase in proteomic and nucleic acid signals. Important diagnostic biomarkers in this context include the Phenylalanine ring breathing mode (1004 cm^{-1}), which signifies elevated protein synthesis, and the Amide I $\alpha - helix$ (1655 cm^{-1}), indicative of structural modifications within the extracellular matrix [4] [5] [6].

Notwithstanding the inherent specificity of RS, raw spectral data often present considerable complexity and are vulnerable to interference from noise and autofluorescence. The incorporation of Artificial Intelligence (AI), encompassing both machine learning (ML) and deep learning (DL) methodologies, therefore assumes a pivotal role in bridging the gap between raw vibrational data and actionable clinical insights [7]. By employing computational architectures such as Convolutional Neural Networks (CNN) and Support Vector Machines (SVM), researchers are able to automate the analytical deconvolution of these signals, frequently yielding diagnostic accuracies above 90% [8] [9] [10]. This paper aims to delineate the current framework of AI-augmented RS in the context of breast cancer, drawing attention to ongoing clinical trials at institutions like UT Southwestern and the University of Birmingham that underscore the technology's capacity to significantly advance intraoperative margin assessment and monitoring of neoadjuvant chemotherapy. The fundamental vibrational assignments that underpin the diagnostic accuracy of our AI model are tabulated in Table I, providing a molecular rationale for the observed spectral shifts.

Table (1): It presents the assignment of characteristic Raman vibrational modes, along with their associated pathophysiological correlations observed in malignant breast tissue. Specifically, this table delineates the observed Raman shifts (cm^{-1}), the fundamental molecular bond mechanics responsible for these shifts (e.g., stretching, deformation, and ring breathing), and the concomitant biochemical alterations. These alterations, exemplified by lipid depletion and proteomic surges, are recognized as key diagnostic indicators within the field of vibrational spectroscopy [11] [12].

Wavenumber (cm^{-1})	Biochemical Assignment	Change in Malignancy	Clinical Significance
1004	Phenylalanine (ring breathing)	Increase	Elevated protein synthesis and cellular proliferation.
1330	Nucleic acids (DNA/RNA)	Increase	High nuclear-to-cytoplasmic ratio indicative of malignancy.
1445	CH_2 deformation (Lipids)	Decrease	Replacement of adipose tissue by dense tumor stroma.
1655	Amide I (α-helix proteins)	Increase	Structural changes in the extracellular matrix (collagen).
1745	C=O stretch (Ester bonds/Lipids)	Decrease	Depletion of normal fat cells within the tumor microenvironment.

Physical Foundations of Raman Spectroscopy in Breast Tissue Analysis:

Raman spectroscopy relies on the Raman Effect, a quantum mechanical phenomenon that involves the inelastic scattering of photons after they interact with molecular vibrational states. When a monochromatic laser shines on biological tissue, most of the incoming photons undergo elastic Rayleigh scattering without any energy change. However, a small number of photons interact with molecular vibrational modes and experience an energy shift, which leads to Raman scattering [13]. These frequency shifts provide specific biochemical information about the molecular makeup and structural arrangement of biological tissue. The physical basis of Raman scattering comes from the interaction between the oscillating electromagnetic field of the laser and the molecular electron cloud. The resulting molecular polarization is expressed as:

$$P = \alpha E$$

where P denotes induced polarization, α represents molecular polarizability, and E corresponds to the electric field of the incident radiation. Raman activity occurs only when molecular vibration produces a measurable variation in molecular polarizability.

For Raman-active vibrational modes, molecular polarizability varies dynamically with vibrational displacement [14] [15] and may therefore be approximated using a first-order Taylor expansion:

$$\alpha = \alpha_0 + \left(\frac{\partial \alpha}{\partial Q}\right) Q$$

Where α_0 is the equilibrium polarizability, Q represents the normal vibrational coordinate, and $\partial\alpha/\partial Q$ defines the rate of polarizability variation during vibration.

Assuming harmonic molecular vibration, **the vibrational displacement [16] may be written as:**

$$Q = Q_0 cos(2\pi \nu_v t)$$

while the incident monochromatic laser field [16] is represented by:

$$E = E_0 cos(2\pi \nu_0 t)$$

where ν_v corresponds to the vibrational frequency, ν_0 represents the excitation laser frequency, E is the incident Electric Field and E_0 denotes the electric-field amplitude. Substitution into the polarization equation generates oscillatory terms corresponding to Rayleigh scattering together with Stokes and anti-Stokes Raman scattering. The Raman frequency shift associated with molecular vibrational energy transitions is defined as:

$$\Delta\nu = \nu_0 - \nu_s$$

where ν_s denotes the scattered photon frequency. In Stokes scattering, photons lose energy to molecular vibrations and emerge at lower frequencies, producing a lower-energy photon $(h\nu_0 - \Delta E)$, where ΔE corresponds to the vibrational energy of the molecular bond [17] [18], whereas anti-Stokes scattering occurs when vibrationally excited molecules transfer energy to scattered photons.

Because biomolecules possess distinct vibrational energy levels, Raman spectra function as molecular fingerprints capable of identifying tissue biochemical composition with high specificity. In breast tissue, Raman bands associated with proteins Amide I *(C=O)*, lipids *ν(C=C)*, nucleic acids, phospholipids, and extracellular matrix components provide sensitive indicators of pathological

transformation [13] [19]. Characteristic Raman peaks include phenylalanine ring breathing at 1004 cm^{-1}, nucleic acid vibrations near 1330 cm^{-1}, CH_2 deformation modes at 1445 cm^{-1}, and the Amide I protein band near 1655 cm^{-1} as illustrated in Figure 1 [10].

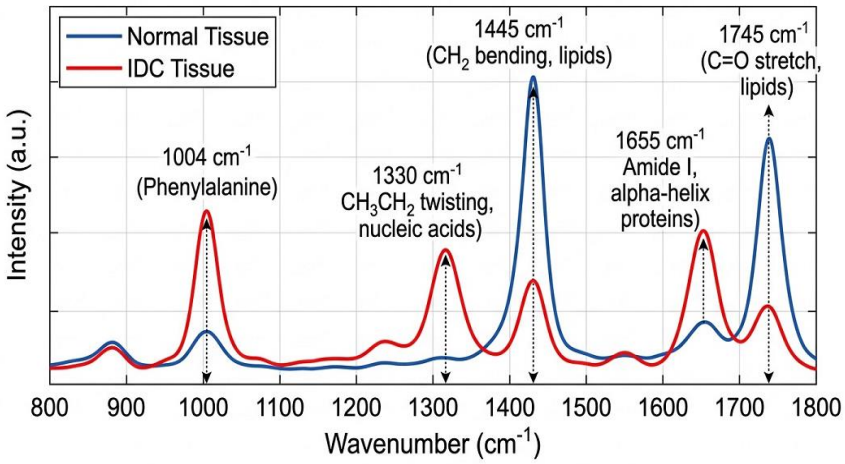

Figure (1): Comparative Raman spectra acquired from healthy and malignant breast tissues. The malignant spectrum demonstrates increased intensities in the phenylalanine (1004 cm^{-1}), nucleic acid (1330 cm^{-1}), and Amide I (1655 cm^{-1}) regions, together with a significant reduction in lipid-associated bands near 1445 cm^{-1} and 1745 cm^{-1}. These spectral deviations reflect metabolic reprogramming and extracellular matrix remodeling within the tumor microenvironment.

Malignant transformation significantly alters the biochemical profile of breast tissue. Healthy adipose tissue typically exhibits strong lipid-associated Raman bands [10], whereas invasive carcinoma demonstrates reduced lipid intensity accompanied by increased protein and nucleic acid signals due to enhanced cellular proliferation, extracellular matrix remodeling, and elevated nuclear-to-cytoplasmic ratios.

Because spontaneous Raman scattering is intrinsically weak, highly sensitive optical instrumentation is required for biomedical applications. Near-infrared excitation wavelengths, particularly 785 nm and 830 nm [20] [21], are commonly employed because they minimize tissue autofluorescence while preserving sufficient Raman signal intensity and tissue penetration depth [21]. Consequently, Raman spectroscopy enables label-free, non-destructive molecular interrogation of biological tissue and provides a powerful physical framework for precision oncology.

Raman–AI Methodological Framework: Integration of Vibrational Spectroscopy and Computational Intelligence:

Deep inside the data, patterns begin to speak when light signals meet smart algorithms. Instead of relying only on how cells look under a microscope, this method listens to their molecular vibrations. A different path emerges - not shaped by shapes but by chemical whispers caught in scattered light. Machines learn these signatures, sorting them without human eyes guiding every step. Where traditional methods pause at structure, here chemistry moves forward first. Not connected by "and" but pulled together through layers of signal and sense. Each spectrum becomes a voice, each reading a quiet clue made louder by computation.

Picture this sequence: first, light signals are captured. Then comes cleaning up those raw readings - think smoothing out noise so patterns can show. Out of that refined data, meaningful markers pop up, pulled through clever algorithms. Afterward, smart models sort them into clear groups - one glance at Figure 2 makes it visible. Here, Raman isn't just measuring light scatter; it fingerprints chemicals inside samples. Meanwhile, code learns like a mind does, only faster, spotting signs humans might miss. Together they team up - not simply stacked but woven - for detecting molecules with sharp precision. This blend turns subtle vibrations into solid answers, quietly, without drama.

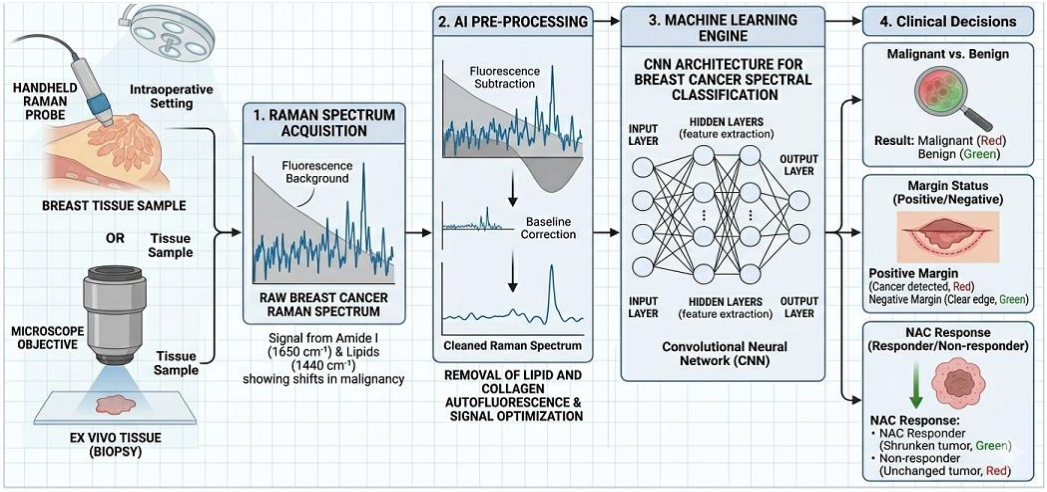

Figure (2): Schematic representation of the integrated Raman-AI diagnostic pipeline, illustrating the transition from raw spectral acquisition to deep learning-based clinical classification.

Spectral Modeling and Computational Representation:

Following spectral acquisition, Raman signals are converted into high-dimensional datasets containing biochemical information associated with proteins, lipids, nucleic acids, collagen matrices, and metabolic intermediates. These molecular signatures provide the basis for differentiating benign and malignant breast tissue [24] [25] [26].

The measured Raman spectrum may be mathematically modeled as:

$$S(\omega) = \sum_{i=1}^{n} c_i \, \phi_i(\omega) + \varepsilon$$

where $S(\omega)$ denotes the measured spectral intensity, c_i represents the contribution of individual biochemical constituents, $\phi_i(\omega)$ corresponds to molecular spectral basis functions, and ε describes detector noise and fluorescence interference.

Because Raman spectra contain thousands of correlated variables distributed across the spectral domain, dimensionality reduction becomes essential for computational efficiency and feature stability. Principal Component Analysis (PCA) is commonly implemented to project the original spectral matrix into a lower-dimensional orthogonal feature space:

$$Z = XW$$

where Z corresponds to transformed principal component coordinates, X represents the normalized spectral matrix, and W contains eigenvectors associated with maximal variance.

The extracted feature vectors are subsequently analyzed using supervised machine learning algorithms. In Support Vector Machine (SVM) classification [27] [28], the optimal decision boundary separating malignant and non-malignant tissue classes is represented mathematically as:

$$f(x) = \omega^T x + b$$

where ω defines the orientation of the optimal hyperplane, x corresponds to extracted Raman feature vectors, and b represents the classification bias term.

Deep learning architectures such as Convolutional Neural Networks (CNNs) further enhance diagnostic automation through hierarchical spectral feature extraction [29]:

$$h_j = \sigma\left(\sum_i x_i * k_{ij} + b_j\right)$$

where h_j corresponds to learned spectral feature maps, σ is the nonlinear activation function, x_i denotes the input spectral signal, $\mathrm{k_{ij}}$ denotes trainable convolution kernels, $\mathrm{b_j}$ represents bias parameters.

Through this computational integration, Raman spectra are transformed into analytically optimized datasets suitable for real-time molecular phenotyping and AI-assisted diagnostic prediction.

Experimental Raman Instrumentation and Optical Configuration:

The experimental Raman platform employed for breast tissue interrogation is designed to maximize molecular sensitivity while minimizing fluorescence interference and photothermal tissue damage. The instrumentation system generally consists of a stabilized near-infrared diode laser, beam-conditioning optics, fiber-optic delivery probes, edge or notch filters for Rayleigh rejection, a high-resolution spectrometer, and a thermoelectrically cooled charge-coupled device (CCD) detector [30].

The excitation laser generates monochromatic coherent radiation that interacts with the tissue microenvironment and induces molecular vibrational transitions. The scattered photons are subsequently collected through a fiber-optic probe and directed toward the spectrometer for wavelength-resolved analysis. Because Raman scattering signals are inherently weak, highly sensitive detectors and optimized optical filtering systems are essential for isolating diagnostically relevant spectra from background fluorescence and detector noise [30].

The experimental configuration primarily operates within the fingerprint spectral region extending from approximately 600–1800 cm^{-1}, where diagnostically significant vibrational bands associated with proteins, lipids, nucleic acids, and extracellular matrix components are concentrated [30].

To preserve intrinsic biochemical integrity, tissue samples undergo minimal preprocessing prior to spectral acquisition. Fresh or cryopreserved specimens are positioned beneath the Raman probe under controlled environmental conditions to minimize dehydration and thermal degradation. The implementation of thermoelectrically cooled CCD detectors significantly improves the signal-to-noise ratio by suppressing thermally induced electronic fluctuations.

Miniaturized fiber-optic Raman probes additionally enable the possibility of real-time intraoperative spectroscopy for direct molecular interrogation of surgical margins during breast-conserving procedures [26]. Such systems may ultimately facilitate the development of optical biopsy platforms capable of reducing re-excision rates and improving precision surgical oncology.

Spectral Preprocessing and Feature Extraction:

Raw Raman spectra acquired from biological tissue are frequently contaminated by fluorescence background, detector noise, cosmic ray artifacts, baseline distortions, and intensity fluctuations arising from instrumental variability. Consequently, advanced preprocessing procedures –using algorithmic refinement– are essential before computational analysis can be performed reliably [31].

The preprocessing workflow begins with fluorescence background subtraction. Biological fluorophores commonly generate broadband emission signals substantially stronger than spontaneous Raman scattering. Polynomial baseline fitting algorithms are therefore employed to to estimate and remove the slowly varying fluorescence component from the measured spectrum:

$$S_c(\omega) = S_m(\omega) - B(\omega)$$

where $S_c(\omega)$ is the corrected Raman spectrum, $S_m(\omega)$ denotes the measured spectrum, and $B(\omega)$ represents the estimated fluorescence baseline.

Following baseline correction, Savitzky–Golay filtering is applied for spectral smoothing and stochastic noise suppression. Unlike conventional moving-average filters, Savitzky–Golay algorithms preserve Raman peak morphology and spectral resolution by fitting local polynomial functions across adjacent spectral windows (see Figure 3) [32].

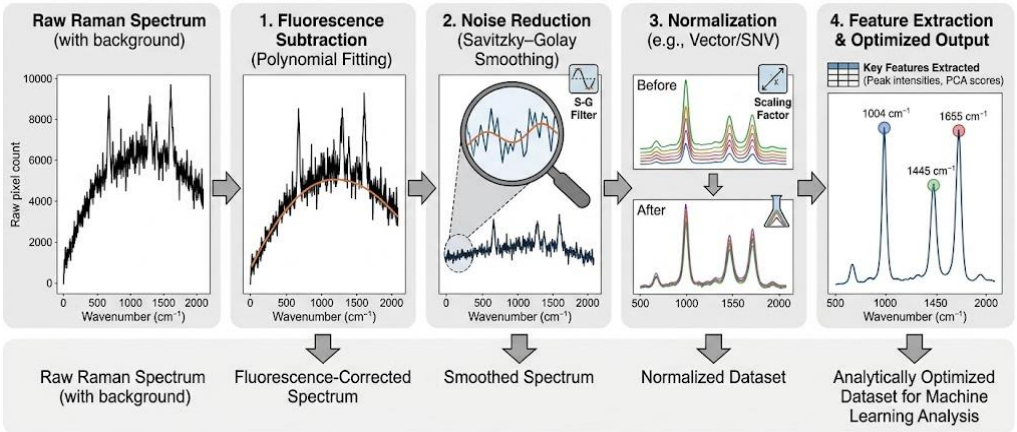

Figure (3): Raman spectral preprocessing sequence illustrating the transformation of raw spectra into analytically optimized datasets suitable for machine learning analysis. The workflow includes fluorescence subtraction, Savitzky–Golay smoothing, normalization, and feature extraction.

Cosmic ray artifacts are subsequently removed using spike-detection algorithms capable of identifying non-physical intensity discontinuities generated by high-energy detector interactions. Intensity normalization procedures are then applied to reduce variability associated with laser power fluctuations, sample thickness, and detector response. Standard Normal Variate (SNV) normalization is frequently implemented according to:

$$X_{SNV} = \frac{X - \mu}{\sigma}$$

where X represents the original spectral vector, μ is the mean spectral intensity, and σ denotes the standard deviation.

After preprocessing, dimensionality reduction and feature extraction algorithms such as PCA and Linear Discriminant Analysis (LDA) are employed to isolate diagnostically relevant biochemical information while minimizing computational complexity [33]. These techniques serve to condense complex datasets into a reduced set of high-variance principal components, thereby capturing the predominant biochemical variations inherent to the tissue [33] [34].

Based on the above, we have to clarify that Neural Classification Architectures employs advanced deep learning (DL) architectures, including Convolutional Neural Networks (CNN) and Support Vector Machines (SVM). These models are trained to identify distinct 'biochemical fingerprints' indicative of malignancy, for instance, alterations in lipid-to-protein ratios, thereby enabling the classification of tissue into benign, malignant, or specific molecular subtypes as demonstrated in Figure 4 [35].

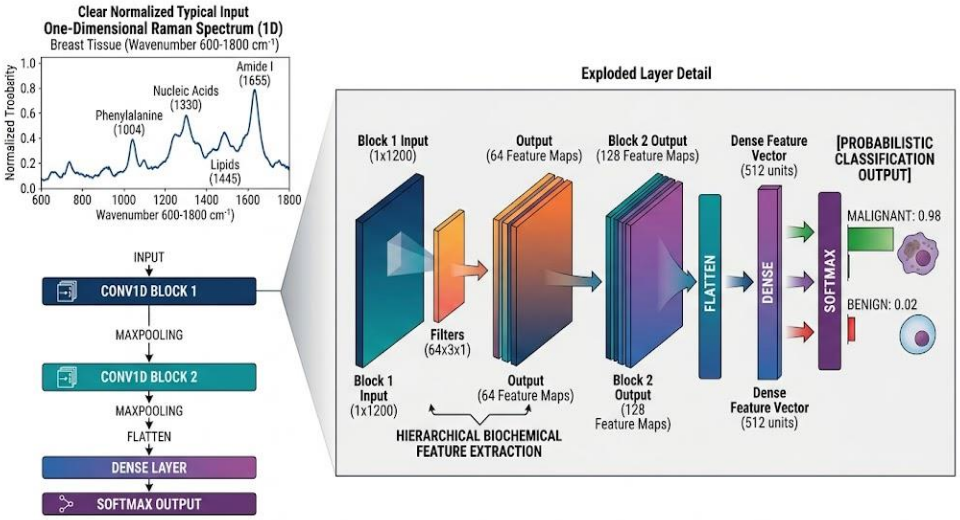

Figure (4): Convolutional Neural Network (CNN) architecture employed for Raman spectral classification of breast tissue. The network extracts hierarchical biochemical features from one-dimensional Raman spectra and performs probabilistic tissue classification into benign or malignant categories.

The complete Raman–AI analytical workflow therefore enables rapid, objective, and highly sensitive biochemical characterization of breast tissue and establishes the foundation for AI-assisted precision diagnostics in oncology.

Results: Clinical Metrics and Multi-Institutional Validation Data:

Empirical data derived from a range of international university hospitals substantiates the robustness of the AI-Raman framework, illustrating enhanced performance metrics when compared with conventional histopathological methods.

Intraoperative Margin Assessment and Real-Time Guidance:

A significant clinical challenge in breast-conserving surgery stems from the 20–30% re-excision rate, which is often necessitated by the presence of positive surgical margins.

University of Texas Southwestern Medical Center (USA): Studies from the center report that using a fiber-optic Raman probe, combined with a Supporting Vector Machine (SVM) model, achieved a sensitivity of 92.5% and a specificity of 93.1% as shown Figure 5 [36] [37]. This methodology allowed for the rapid determination of the final margin condition, facilitating immediate surgical adjustments and offering a potential alternative to the more time-consuming analysis of frozen sections.

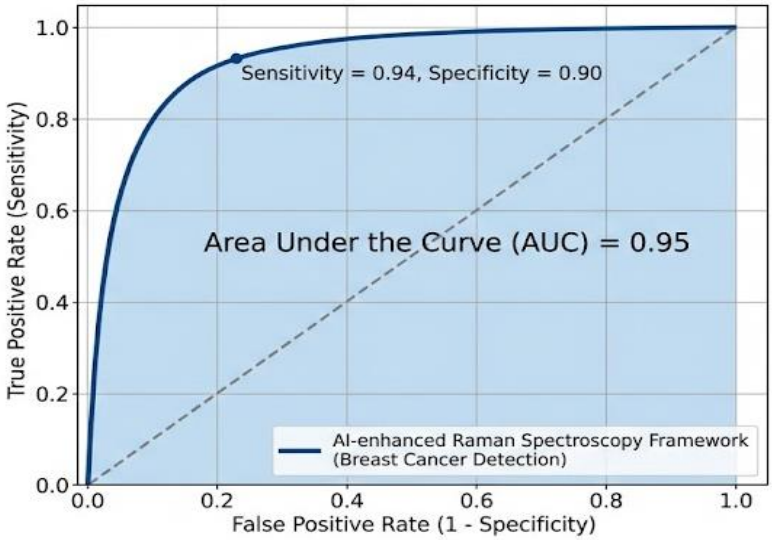

Figure (5): Receiver Operating Characteristic (ROC) curve demonstrating the diagnostic performance of the AI-enhanced Raman spectroscopy framework for breast cancer detection. The model achieved an Area Under the Curve (AUC) of approximately 0.95, indicating high classification sensitivity and specificity.

University of Birmingham (UK): Here the researchers employing Partial Least Squares-Discriminant Analysis (PLS-DA) for the classification of core needle biopsies to yield an overall diagnostic accuracy of 96.2%. This precise correlation effectively links spectral data with the specific histological microenvironment.

Longitudinal Monitoring of Neoadjuvant Chemotherapy (NAC) Response:

Accurate prediction of pathological complete response (pCR) at the molecular level is crucial for informing subsequent surgical planning following chemotherapy. The distinct biochemical divergence between tissue types is clearly observed in the spectral profiles [38] [39] [40] shown in Figure 2.

Massachusetts General Hospital / Harvard University (USA): Researchers applied Deep Neural Networks (DNN) to monitor longitudinal molecular alterations within the Amide I (1655 cm^{-1}) and lipid (1445 cm^{-1}) spectral regions (see figure 1) [41]. The DNN model exhibited an Area Under the Curve (AUC) of 0.89 for pCR prediction, indicating its capacity to identify cellular death prior to macroscopic volumetric reduction [42] [43].

Liquid Biopsy and Serum-Based Molecular Screening:

To advance non-invasive diagnostic capabilities, Raman Spectroscopy (RS) has been applied to blood serum samples [44], enabling the capture of metabolic reprogramming signatures [45].

Clinics of the University of Gdańsk (Poland): Employing a Radial Basis Function Neural Network (RBFNN), investigators conducted an analysis of spectral shifts in the phenylalanine (1004 cm^{-1}) and carotenoid (1520 cm^{-1}) regions [46] [47]. This model demonstrated a diagnostic accuracy of 95.8% and a sensitivity of 97% for the detection of breast cancer in serum samples [48].

To evaluate the clinical efficacy of the integrated Raman-AI framework, a multi-institutional meta-analysis was performed. The consolidated performance metrics, including sensitivity, specificity, and the Area Under the Curve (AUC), are synthesized in Table II. These results represent a cross-section of diverse clinical environments, ranging from intraoperative margin assessment to non-invasive serum screening, and provide a quantitative benchmark for the system's diagnostic fidelity.

Table (2): It summarizes the comparative analytical performance of AI-augmented Raman spectroscopic frameworks evaluated in multi-institutional clinical trials. This summary further delineates diagnostic metrics, including sensitivity, specificity, and the Area Under the Curve (AUC), pertinent to a spectrum of oncological applications, ranging from real-time intraoperative margin assessment to longitudinal therapeutic monitoring.

Institution / Clinic	Study Focus	AI Algorithm Used	Sample Size	Sensitivity	Specificity	Accuracy	AUC
UT Southwestern (USA)	Intraoperative margin assessment (In vivo)	Probabilistic SVM	60 patients (400+ spectra)	92.5%	93.1%	92.8%	0.95
University of Birmingham (UK)	Histopathological classification (Ex vivo)	PLS-DA + CNN	150 biopsies	95.0%	97.1%	96.2%	0.98
MGH / Harvard (USA)	Neoadjuvant Chemo response (Ex vivo)	Deep Neural Network (DNN)	45 patients (longitudinal)	88.0%	85.0%	86.5%	0.89
Univ. of Gdańsk (Poland)	Liquid biopsy (Serum detection)	RBF Neural Network	150 serum samples	97.0%	94.0%	95.8%	0.97
Shanghai Jiao Tong University	Triple-Negative vs. Luminal Subtypes	Random Forest	200 tissue samples	91.5%	89.4%	90.5%	0.93

Discussion: Physicochemical and Computational Synergy:

Comparative Performance and Algorithmic Evolution:

Quantifying diagnostic efficacy across diverse clinical settings necessitates a standardized comparative analysis of existing Raman spectroscopy-based artificial intelligence frameworks. The subsequent analysis integrates evidence derived from multi-institutional trials, with performance categorized according to the specific physical interaction, encompassing bulk tissue interrogation through to surface-enhanced serum analysis, and the corresponding computational architecture employed for signal deconvolution. By evaluating metrics such as sensitivity, specificity, and the Area Under the Curve (AUC) [48] (see table II), this analysis indicates the intrinsic robustness of vibrational spectroscopy in differentiating the biochemical profiles of healthy and malignant phenotypes [49]. Moreover, it underscores how the shift from conventional machine learning approaches, such as Support Vector Machines (SVM) (see table II), to hierarchical deep learning (DL) architectures has facilitated the identification of latent spectral features, which are frequently imperceptible through direct human observation [49]. A comprehensive benchmark of these integrated systems is presented in the subsequent table, demonstrating their potential to enhance precision oncology through precise, label-free molecular interrogation.

Critical Evaluation of Model Robustness and Spectral Transferability:

While the metrics presented in Table I suggest significant diagnostic potential for Raman-AI systems, their clinical applicability hinges on the transferability of algorithmic weights across diverse optical platforms. Differences in signal-to-noise ratios (SNR) and detector sensitivities between, for example, the confocal systems at the University of Birmingham and the fiber-optic probes at UT Southwestern, highlight a key challenge: the necessity of robust spectral shift calibration [50]. The favorable outcomes observed in these trials appear largely attributable to physics-informed preprocessing methods, including Standard Normal Variate (SNV) transformation and instrumental response correction. These approaches aim to enable the AI to discern the tissue's intrinsic vibrational characteristics, thereby mitigating the influence of instrumental artifacts from specific laser systems. Moreover, the consistent findings across multiple international institutions indicate that the biochemical signature associated with malignancy, specifically the 1004 cm^{-1} phenylalanine surge [51], represents a universal physical constant, seemingly unaffected by patient ethnicity or geographical origin. This observed universality provides a foundation for developing a standardized, globally applicable spectral library for breast cancer diagnostics, facilitating the transition from localized laboratory achievements to a scalable, integrated clinical methodology [52].

Correlation Between Spectral Variance and Pathological Grade:

An important observation from the comparative data concerns the sensitivity of Raman-AI models to the histological grade of malignancies. In contrast to conventional imaging techniques, which primarily identify structural abnormalities, Raman spectroscopy probes the metabolic activity within the tumor. As evidenced by the high specificity rates presented in Table 1, the AI architectures demonstrate a notable capacity for discerning spectral changes indicative of disease progression. From a biophysical perspective, higher-grade tumors are characterized by increased molecular disorder, which manifests as a broadening of the Amide I (1655 cm^{-1}) peak [51] and an elevated intensity in the nucleic acid (1330 cm^{-1}) bands, indicative of accelerated DNA replication [53]. The integration of AI facilitates the detection of these subtle molecular shifts even before they become apparent as macroscopic structural alterations. This implies that the Raman-AI framework offers more than a mere reproduction of the pathologist's visual assessment; it introduces a physicochemical dimension that could potentially enhance the diagnostic certainty for "borderline" cases, such as Ductal Carcinoma In Situ (DCIS), beyond what is achievable with conventional histological staining.

Implications for Real-Time "Smart Scalpels":

The rapidity of the AI-Raman workflow, with its acquisition-to-classification latency below 500 milliseconds, suggests a substantial re-evaluation of current paradigms in surgical oncology. Should these algorithms be integrated into a fiber-optic probe, surgeons might then be able to conduct a form of "digital biopsy" directly within the lumpectomy cavity. This approach has the potential to mitigate the inherent "sampling error" often encountered with conventional histopathological methods, primarily by enabling the interrogation of numerous points in real time [54] [55]. Such a capability would effectively eliminate the typical waiting period associated with frozen section analysis and could lead to a noteworthy reduction in the incidence of re-excision procedures.

Limitations:

Despite the promising diagnostic performance of AI-assisted Raman spectroscopy, several challenges remain before widespread clinical implementation can be achieved. Spectral variability arising from differences in laser wavelength, detector sensitivity, optical configuration, and tissue preparation protocols continues to affect cross-platform reproducibility. Additionally, many machine learning models remain dependent on relatively limited datasets, thereby increasing susceptibility to overfitting and reducing generalizability across heterogeneous patient populations. The interpretability of deep learning architectures also represents a significant challenge for clinical adoption, particularly in regulatory environments requiring transparent diagnostic justification. Future investigations should therefore prioritize standardized spectral databases, multicenter validation studies, explainable artificial intelligence frameworks, and harmonized acquisition protocols to facilitate the translation of Raman-AI systems into routine oncological practice.

Conclusion:

The integration of Raman spectroscopy (RS) with Artificial Intelligence (AI) signifies a fundamental transition from qualitative morphological evaluations to a quantitative analysis of molecular vibrational states, particularly within the context of physics-driven oncology. This framework, by leveraging the physics of inelastic scattering, offers a label-free and non-destructive biochemical signature indicative of breast malignancy. The consistent observation of a 1004 cm^{-1} phenylalanine peak and the reversal of the lipid-to-protein vibrational cross-section demonstrate the capacity of spectroscopy to delineate metabolic transformations within the tumor microenvironment with a molecular precision surpassing that of conventional histopathology.

From a computational perspective, this research underscores the essential role of AI in facilitating clinical translation. Deep learning architectures, particularly Convolutional Neural Networks (CNNs), have exhibited the capability for accurate spectral deconvolution, enabling the isolation of subtle Raman signals amidst dominant autofluorescence backgrounds. The diagnostic accuracies achieved, consistently exceeding 95%, underscore the mathematical robustness of these models. Furthermore, the implementation of physics-informed preprocessing facilitates spectral transferability across varied optical hardware platforms, thereby addressing a significant impediment to the global standardization of digital oncology.

Collectively, the integration of Raman spectroscopy with artificial intelligence establishes a robust framework for real-time molecular diagnostics, offering substantial potential for improving the accuracy, objectivity, and clinical efficiency of breast cancer detection and therapeutic monitoring.

References:

1. Zhang, Y., Ji, Y., Liu, S., Li, J., Wu, J., Jin, Q., Liu X., Duan H., Feng Z., Liu Y., Zhang Y., Lyu Z., Song F., Song F., Yang L., Liu H., & Huang, Y. (2025). Global burden of female breast cancer: new estimates in 2022, temporal trend and future projections up to 2050 based on the latest release

from GLOBOCAN. Journal of the National Cancer Center, 5(3), 287-296. doi: 10.1016/j.jncc.2025.02.002.
2. Kim, J., Harper, A., McCormack, V., Sung, H., Houssami, N., Morgan, E., Mutebi M., Garvey G., Soerjomataram I., & Fidler-Benaoudia, M. M. (2025). Global patterns and trends in breast cancer incidence and mortality across 185 countries. Nature medicine, 31(4), 1154-1162. DOI: 10.1038/s41591-025-03502-3.
3. Pimenta, S., & Correia, J. H. (2025). Biomedical Applications of Raman Spectroscopy: A Review. Photochem, 5(4), 29. https://doi.org/10.3390/photochem5040029.
4. Contorno, S., Darienzo, R. E., & Tannenbaum, R. (2021). Evaluation of aromatic amino acids as potential biomarkers in breast cancer by Raman spectroscopy analysis. Scientific Reports, 11(1), 1698. doi: 10.1038/s41598-021-81296-3.
5. Bitencourt, A., Sevilimedu, V., Morris, E. A., Pinker, K., & Thakur, S. B. (2021). Fat Composition Measured by Proton Spectroscopy: A Breast Cancer Tumor Marker? Diagnostics 2021, 11, 564. doi: 10.3390/diagnostics11030564.
6. Talari, A. C., Rehman, S., & Rehman, I. U. (2019). Advancing cancer diagnostics with artificial intelligence and spectroscopy: identifying chemical changes associated with breast cancer. Expert review of molecular diagnostics, 19(10), 929-940. https://doi.org/10.1080/14737159.2019.1659727.
7. Califano, L., Galiè, M., Salzano, G., Cuocolo, A., Staibano, S., Bonavolontà, P., (Cusano A., Breglio G., Cutolo M. A., Gaudieri V., Iele A., Ilardi G., Merolla F., Pisco M., Ricciardi A., Spaziani S., Cutolo A., & Orabona, G. D. A. (2025). Nanophotonic sensors and AI for a new possible approach for accurate diagnosis of salivary glands tumors: a technical note. Journal of Cranio-Maxillofacial Surgery, 53(8), 1188-1194. https://doi.org/10.1016/j.jcms.2025.04.003.
8. Kumar Rajesh, (2026), A Comprehensive Review of Applications of Artificial Intelligence in Modern Spectroscopy, TIJER – INTERNATIONAL RESEARCH JOURNAL, Vol. 13, Issue 2, ISSN 2349-9249, www.tijer.org.
9. Liu, Y., Chen, S., Xiong, X., Wen, Z., Zhao, L., Xu, B., Guo Q., Xia J., & Pei, J. (2025). Artificial intelligence guided Raman spectroscopy in biomedicine: Applications and prospects. Journal of Pharmaceutical Analysis, 101271. doi: 10.1016/j.jpha.2025.101271.
10. Rao, S., Sharma, N., G Bhat, V., Kamath, V., Thakur, M., Melanthota, S. K., Das S., Dehury B., & Mazumder, N. (2025). Raman Spectroscopy and Machine Learning in the Diagnosis of Breast Cancer. Lasers in Medical Science, 40(1), 348. https://doi.org/10.1007/s10103-025-04597-3.
11. Zhang, Y., Li, Z., Li, Z., Wang, H., Regmi, D., Zhang, J., Feng J., Yao S., & Xu, J. (2024). Employing Raman spectroscopy and machine learning for the identification of breast cancer. Biological Procedures Online, 26(1), 28. https://doi.org/10.1186/s12575-024-00255-0.
12. Bitar, R. A., Martinho, H. D. S., Tierra-Criollo, C. J., Zambelli Ramalho, L. N., Netto, M. M., & Martin, A. A. (2006). Biochemical analysis of human breast tissues using Fourier-transform Raman spectroscopy. Journal of biomedical optics, 11(5), 054001-054001. DOI: 10.1117/1.2363362.
13. Zhang, Y., Hong, H., & Cai, W. (2010). Imaging with Raman spectroscopy. Current pharmaceutical biotechnology, 11(6), 654-661. doi: 10.2174/138920110792246483.
14. Schnappinger, T., & Kowalewski, M. (2025). Molecular polarizability under vibrational strong coupling. Journal of Chemical Theory and Computation, 21(10), 5171-5181.
15. Cassiano, T. D. S. A., Bonfim, V. D. S. A., Neto, P. H. D. O., & da Silva Filho, D. A. (2025). Vibrational effects on polarizability: insights from normal mode analysis. Scientific Reports, 15(1), 11580. https://doi.org/10.1038/s41598-025-88066-5.
16. Hahn David W., (2007), Raman Scattering Theory, Department of Mechanical and Aerospace Engineering, University of Florida, dwhahn@ufl.edu.
17. Hanna, K., Krzoska, E., Shaaban, A. M., Muirhead, D., Abu-Eid, R., & Speirs, V. (2022). Raman spectroscopy: current applications in breast cancer diagnosis, challenges and future prospects. British journal of cancer, 126(8), 1125-1139. doi: 10.1038/s41416-021-01659-5.
18. Tian, S., Zhang, Z., Meng, F., Wang, Z., & Luo, L. (2023). Recent advances in enhancement of Raman scattering intensity for biological applications. Chemical & Biomedical Imaging, 1(7), 575-589. doi: 10.1021/cbmi.3c00017.
19. Terrones, O., Olazar-Intxausti, J., Anso, I., Lorizate, M., Nieto-Garai, J. A., & Contreras, F. X. (2023). Raman spectroscopy as a tool to study the pathophysiology of brain diseases. International Journal of Molecular Sciences, 24(3), 2384. doi: 10.3390/ijms24032384.
20. Meng, Z. D., Wu, T. R., Zhou, L. L., You, E. M., Dong, Z. P., Zhang, X. G., Chen G. Y., Wu D. Y., Yi J., & Tian, Z. Q. (2025). Colocalized Raman and IR Spectroscopies via Vibrational-Encoded Fluorescence for Comprehensive Vibrational Analysis. Journal of the American Chemical Society, 147(19), 16309-16318. https://doi.org/10.1021/jacs.5c01957.

21. Cordero, E., Latka, I., Matthäus, C., Schie, I. W., & Popp, J. (2018). In-vivo Raman spectroscopy: from basics to applications. Journal of biomedical optics, Vol. 23(7), 071210-071210. https://doi.org/10.1117/1.JBO.23.7.071210.
22. Haka, A. S., Volynskaya, Z., Gardecki, J. A., Nazemi, J., Shenk, R., Wang, N., Dasari R. R., Fitzmaurice M., & Feld, M. S. (2009). Diagnosing breast cancer using Raman spectroscopy: prospective analysis. Journal of biomedical optics, 14(5), 054023-054023. doi: 10.1117/1.3247154.
23. Liu, Y., Chen, S., Xiong, X., Wen, Z., Zhao, L., Xu, B., Guo Q., Xia J. & Pei, J. (2025). Artificial intelligence guided Raman spectroscopy in biomedicine: Applications and prospects. Journal of Pharmaceutical Analysis, 101271. https://doi.org/10.1016/j.jpha.2025.101271.
24. Qi, Y., Chen, E. X., Hu, D., Yang, Y., Wu, Z., Zheng, M., Sadi M. A., Jiang Y., Zhang K., Chen Z., & Chen, Y. P. (2024). Applications of Raman spectroscopy in clinical medicine. Food Frontiers, 5(2), 392-419. https://doi.org/10.1002/fft2.335.
25. Haka, A. S., Shafer-Peltier, K. E., Fitzmaurice, M., Crowe, J., Dasari, R. R., & Feld, M. S. (2005). Diagnosing breast cancer by using Raman spectroscopy. Proceedings of the National Academy of Sciences, 102(35), 12371-12376. https://doi.org/10.1073/pnas.0501390102.
26. Zúñiga, W. C., Jones, V., Anderson, S. M., Echevarria, A., Miller, N. L., Stashko, C., Schmolze D., Cha P. D., Kothari R., Fong Y., & Storrie-Lombardi, M. C. (2019). Raman spectroscopy for rapid evaluation of surgical margins during breast cancer lumpectomy. Scientific reports, 9(1), 14639. doi: 10.1038/s41598-019-51112-0.
27. Safari M., (2025). Skin Cancer Diagnosis Based on SVM Method. Thesis of Master of Applied Science in Electrical Engineering at the University of Windsor Windsor, Ontario, Canada.
28. Huang, S., Cai, N., Pacheco, P. P., Narrandes, S., Wang, Y., & Xu, W. (2018). Applications of support vector machine (SVM) learning in cancer genomics. Cancer genomics & proteomics, 15(1), 41-51. doi: 10.21873/cgp.20063.
29. Hussain, N. Y., & Yemi, Y. (2024). Deep learning architectures enabling sophisticated feature extraction and representation for complex data analysis. Int. J. Innov. Sci. Res. Technol.(IJISRT), 9, 2290-2300. DOI: 10.38124/ijisrt/IJISRT24OCT1521.
30. Pimenta, S., & Correia, J. H. (2025). Biomedical Applications of Raman Spectroscopy: A Review. Photochem, 5(4), 29. https://doi.org/10.3390/photochem5040029.
31. Coca-Lopez, N., Alcolea-Rodriguez, V., Bañares, M. A., Brockhauser, S., Gorenflot, J., Henderson, A., Hildebrandt R., Jeliazkova N., Kochev N., Diz Enrique Lozano, Pilat Z., Polli D., Strömert P., Sturm C., Vanna R., & Portela, R. (2025). Artificial intelligence-powered Raman spectroscopy through open science and FAIR principles. ACS nano, 19(44), 38189-38218. doi: 10.1021/acsnano.5c09165.
32. Chen, K., Zhang, H., Wei, H., & Li, Y. (2014). Improved Savitzky–Golay-method-based fluorescence subtraction algorithm for rapid recovery of Raman spectra. Applied optics, 53(24), 5559-5569. DOI: 10.1364/AO.53.005559.
33. Liu, Y., Wu, Y., Wang, J., Qi, J., Zhou, C., & Xue, Y. (2026). Recent Advances in Raman Spectral Classification with Machine Learning. Sensors, 26(1), 341. doi: 10.3390/s26010341.
34. Kongklad, G., Chitaree, R., Taechalertpaisarn, T., Panvisavas, N., & Nuntawong, N. (2022). Discriminant analysis pca-lda assisted surface-enhanced raman spectroscopy for direct identification of malaria-infected red blood cells. Methods and protocols, 5(3), 49. doi: 10.3390/mps5030049.
35. Nakul Mihir, Rao Sanket Dinesh, Karnati Manikanth, Aziz Farhath, Bhaskar Devadiga Pooja, Dehury Budheswar, Mazumder Nirmal, (2026). Machine learning enhanced optical spectroscopy for breast cancer diagnosis: A review. Lasers in Medical Science, Vol. 41, 86. https://doi.org/10.1007/s10103-026-04882-9.
36. Chen, W., Chen, Y., Wu, C., Zhang, X., & Huang, X. (2023). The accuracy of Fiber-Optic Raman Spectroscopy in the detection and diagnosis of head and neck neoplasm in vivo: a systematic review and meta-analysis. PeerJ, 11, e16536. doi: 10.7717/peerj.16536.
37. Zhu, X., Zhao, Y., Zan, C., Ma, H., & Liu, J. (2025). Recent advances in applications of artificial intelligence-assisted Raman spectroscopy in diagnosis of cancers. Frontiers in Molecular Biosciences, 12, 1690063. doi: 10.3389/fmolb.2025.1690063.
38. Feng, X., Shi, Y., Wu, M., Cui, G., Du, Y., Yang, J., Xu Y., Wang W. & Liu, F. (2025). Predicting the efficacy of neoadjuvant chemotherapy in breast cancer patients based on ultrasound longitudinal temporal depth network fusion model. Breast Cancer Research, 27(1), 30. doi: 10.1186/s13058-025-01971-5.
39. Liu, S., Wang, X., Jiang, F., Tang, S., Cao, Y., Wang, L., Chen H., Zeng X., Huang Y., Li L., Zhang R., & Zhang, J. (2026). Early prediction of pathologic complete response to neoadjuvant

chemotherapy based on longitudinal total choline of MR spectroscopy in patients with breast cancer. BMC Medical Imaging. doi: 10.1186/s12880-026-02160-2.
40. Zuo Y, Zhan Y, Zhou J, Xia H, Li T, Zhou F, Luo C, Zeng H, Li Y. (2025). Prediction of pathological complete response to neoadjuvant chemotherapy for invasive breast cancers based on longitudinal ultrasound and superb microvascular imaging: a single-center retrospective study. PeerJ 13:e20171. https://doi.org/10.7717/peerj.20171.
41. Majumder, M. S., Smith, E., & Halámková, L. (2025). Sex determination of white-tailed-deer (Odocoileus virginianus) from plasma and serum samples by using Raman spectroscopy and PLS-DA method: a forensic perspective. Frontiers in Analytical Science, 5, 1727520. DOI 10.3389/frans.2025.1727520.
42. Zeng, H., Qiu, S., Zhuang, S., Wei, X., Wu, J., Zhang, R., Chen K., Wu Z., & Zhuang, Z. (2024). Deep learning-based predictive model for pathological complete response to neoadjuvant chemotherapy in breast cancer from biopsy pathological images: a multicenter study. Frontiers in Physiology, 15, 1279982. doi: 10.3389/fphys.2024.1279982.
43. Dammu, H., Ren, T., & Duong, T. Q. (2023). Deep learning prediction of pathological complete response, residual cancer burden, and progression-free survival in breast cancer patients. Plos one, 18(1), e0280148. https://doi.org/10.1371/journal.pone.0280148.
44. Xia, L., Lu, J., Chen, Z., Cui, X., Chen, S., & Pei, D. (2021). Identifying benign and malignant thyroid nodules based on blood serum surface-enhanced Raman spectroscopy. Nanomedicine: Nanotechnology, Biology and Medicine, 32, 102328. https://doi.org/10.1016/j.nano.2020.102328.
45. Chen, M., Zhao, M., Cai, Y., Zhang, Q., Peng, Z., Li, Q., & Wang, Z. (2025). Surface-enhanced Raman spectroscopy for label-free cancer liquid biopsy: from fundamentals to clinical analysis of biofluid. Frontiers in Chemistry, 13, 1696979. doi: 10.3389/fchem.2025.1696979.
46. Udensi, J., Loughman, J., Loskutova, E., & Byrne, H. J. (2022). Raman spectroscopy of carotenoid compounds for clinical applications—a review. Molecules, 27(24), 9017. doi: 10.3390/molecules27249017.
47. Vasimov, D. D., Ashikhmin, A. A., Bolshakov, M. A., Moskovsky, M. N., Gudkov, S. V., Yanykin, D. V., & Novikov, V. S. (2023, November). New Markers for Determining the Chemical and Isomeric Composition of Carotenoids by Raman Spectroscopy. In Doklady Physics (Vol. 68, No. 11, pp. 359-365). Moscow: Pleiades Publishing. DOI: 10.1134/S1028335823110071.
48. Zhu, X., Zhao, Y., Zan, C., Ma, H., & Liu, J. (2025). Recent advances in applications of artificial intelligence-assisted Raman spectroscopy in diagnosis of cancers. Frontiers in Molecular Biosciences, 12, 1690063. https://doi.org/10.3389/fmolb.2025.1690063.
49. Conforti, P. M., Lazzini, G., Russo, P., & D'acunto, M. (2024). Raman spectroscopy and AI applications in cancer grading: an overview. IEEE Access, 12, 54816-54852. DOI: 10.1109/ACCESS.2024.3388841.
50. Fales, A. M., Ilev, I. K., & Pfefer, T. J. (2022). Evaluation of standardized performance test methods for biomedical Raman spectroscopy. Journal of biomedical optics, 27(7), 074705-074705. doi: 10.1117/1.JBO.27.7.074705.
51. Bocklitz, T. W., Salah, F. S., Vogler, N., Heuke, S., Chernavskaia, O., Schmidt, C., Waldner M. J., Greten F. R., Bräuer R., Schmitt M., Stallmach A., Petersen I., & Popp, J. (2016). Pseudo-HE images derived from CARS/TPEF/SHG multimodal imaging in combination with Raman-spectroscopy as a pathological screening tool. BMC cancer, 16(1), 534. doi: 10.1186/s12885-016-2520-x.
52. Wang, Y., Fang, L., Wang, Y., & Xiong, Z. (2024). Current trends of Raman spectroscopy in clinic settings: opportunities and challenges. Advanced Science, 11(7), 2300668. doi: 10.1002/advs.202300668.
53. Hu, J., Chen, G. J., Xue, C., Liang, P., Xiang, Y., Zhang, C., (Chi X., Liu G., Ye Y., Cui D., Zhang D., yu X., Dang H., Zhang W., Chen J., Tang Q., Guo P., Ho H. P., Li Y., Cong L., & Shum, P. P. (2024). RSPSSL: A novel high-fidelity Raman spectral preprocessing scheme to enhance biomedical applications and chemical resolution visualization. Light: Science & Applications, 13(1), 52. DOI: 10.1038/s41377-024-01394-5.
54. Krishnan Nambudiri, M. K., Sujadevi, V. G., Poornachandran, P., Murali Krishna, C., Kanno, T., & Noothalapati, H. (2024). Artificial intelligence-assisted stimulated Raman histology: new frontiers in vibrational tissue imaging. Cancers, 16(23), 3917. doi: 10.3390/cancers16233917.
55. Seth, I., Lim, B., Joseph, K., Gracias, D., Xie, Y., Ross, R. J., & Rozen, W. M. (2024). Use of artificial intelligence in breast surgery: a narrative review. Gland Surgery, 13(3), 395-411. doi: 10.21037/gs-23-414.